

Article

The Preparation of Cu-g-C₃N₄/AC Catalyst for Acetylene Hydrochlorination

Wenli Zhao ¹, Mingyuan Zhu ^{1,2,*} and Bin Dai ^{1,2,*}

¹ School of Chemistry and Chemical Engineering of Shihezi University, Shihezi 832000, Xinjiang, China; zhaowenli@stu.shzu.edu.cn

² Key Laboratory for Green Processing of Chemical Engineering of Xinjiang Bingtuan, Shihezi 832000, Xinjiang, China

* Correspondence: zhumin yuan@shzu.edu.cn (M.Z.); db_tea@shzu.edu.cn (B.D.); Tel.: +86-993-2057277 (M.Z. & B.D.)

Academic Editors: Shaobin Wang and Xiaoguang Duan

Received: 29 September 2016; Accepted: 29 November 2016; Published: 5 December 2016

Abstract: A novel catalyst based on g-C₃N₄/activated carbon was prepared by adding CuCl₂. The catalytic performance of the as-prepared catalyst was investigated in the acetylene hydrochlorination reaction. X-ray photoelectron spectroscopy, temperature programmed desorption, low temperature N₂ adsorption/desorption (Brunauer–Emmett–Teller), and thermal gravity analysis showed that Cu-g-C₃N₄/AC significantly enhanced the catalytic performance of the original catalyst by increasing the relative pyrrolic N content. Cu-g-C₃N₄/AC also affected the adsorption of hydrogen chloride and acetylene, as well as inhibited the coke deposition during acetylene hydrochlorination.

Keywords: acetylene hydrochlorination; non-mercury catalyst; copper

1. Introduction

The use of plastic products is increasing to date. Polyvinyl chloride (PVC) has become the second most frequently used general plastic worldwide. Vinyl chloride monomer (VCM) is used for PVC synthesis. In China, use of acetylene as a raw material to produce VCM still dominates local practices [1]. Mercuric chloride (HgCl₂) supported on activated carbon (AC) is used as the catalyst in the current industrial production process. This approach holds major shortcomings: the catalyst loses volatile active components during the reaction, while its high toxicity is harmful to human health and seriously pollutes the environment. On the other hand, the catalyst cannot generally be reactivated after deactivation. To achieve the efficient and clean production of VCM, the development of new non-mercury catalyst must be urgently addressed [2].

Numerous attempts have been made to develop a non-mercury catalyst, and precious metal catalysts have attracted the attention of researchers, especially the gold-containing catalyst. Hutchings et al. [3] studied the catalytic mechanism of the Au catalyst and found that the activity of acetylene hydrochlorination was improved by adding adsorbed hydrogen chloride (HCl). The authors also noted that the increase in acetylene (C₂H₂) adsorption can deactivate the catalyst. Specifically, HCl adsorption is the reaction rate control step. Li et al. [4] discovered that the enhanced catalytic performance could be attributed to the introduction of polypyrrole (PPy) into multiwall carbon nanotubes (MWCNTs), which increased the adsorption of HCl. Consequently, AuCl₃/PPy-MWCNT demonstrated excellent catalytic performance compared with AuCl₃/MWCNT during acetylene hydrochlorination. However, the price and stability of the Au-based catalyst limit the widespread use of this catalyst [5].

Carbon nitride material has recently attracted attention because of its excellent chemical stability and unique semiconductor band structure. Thus, carbon nitride material has been widely used for

photolysis of aquatic hydrogen, which produces oxygen; light-catalyzed organic synthesis and the photocatalytic degradation of organic pollutants [6,7]. Dai et al. [8] searched for a graphitic carbon nitride catalyst ($g\text{-C}_3\text{N}_4/\text{AC}$), their study revealed that the nitrogen atom of the $g\text{-C}_3\text{N}_4/\text{AC}$ catalyst is the active site for the HCl; thus, the prepared $g\text{-C}_3\text{N}_4/\text{AC}$ catalyst displayed considerable catalytic performance. However, this catalyst rapidly deactivates given its poor stability. This catalyst entails further study.

To solve the high cost and rapid deactivation of catalyst, we introduced the non-precious metal CuCl_2 to the $g\text{-C}_3\text{N}_4/\text{AC}$ catalyst by a simple preparation method. The properties of this new catalyst were explored by acetylene hydrochlorination. Characterization confirmed the success of material preparation; the test results showed that the catalyst possessed good catalytic activity, thereby promoting further research on experimental and theoretical references.

2. Results and Discussion

2.1. Catalytic Performance

The catalytic activities of $g\text{-C}_3\text{N}_4/\text{AC}$ and $\text{Cu-}g\text{-C}_3\text{N}_4/\text{AC}$ are shown in Figure 1. Reaction conditions were as follows: temperature (T) = 180 °C; C_2H_2 hourly space velocity (GHSV) = 72 h^{-1} ; Feed volume ratio $V(\text{HCl})/V(\text{C}_2\text{H}_2) = 1.15$. As a carrier of acetylene hydrochlorination reaction, AC exhibited an initial activity of up to 45%, which declined to 20% after 450 min of reaction (Figure 1a). Under the same conditions, the acetylene conversion of the $g\text{-C}_3\text{N}_4/\text{AC}$ catalyst decreased from 67% to 55% after 450 min of reaction. Therefore, the $g\text{-C}_3\text{N}_4/\text{AC}$ catalyst enhanced the acetylene hydrochlorination reaction to some extent compared to AC. The acetylene conversion by the $\text{Cu-}g\text{-C}_3\text{N}_4/\text{AC}$ catalyst reached 79%, and remained almost constant after 450 min of reaction. Figure 1b displays the selectivity to vinyl chloride in the acetylene hydrochlorination reaction, where the selectivity to VCM of the $g\text{-C}_3\text{N}_4/\text{AC}$ and $\text{Cu-}g\text{-C}_3\text{N}_4/\text{AC}$ catalyst exceed 99.5%. The above-mentioned results show that $g\text{-C}_3\text{N}_4/\text{AC}$ has better catalytic activity, and $\text{Cu-}g\text{-C}_3\text{N}_4/\text{AC}$ catalytic performance is further improved compared with AC.

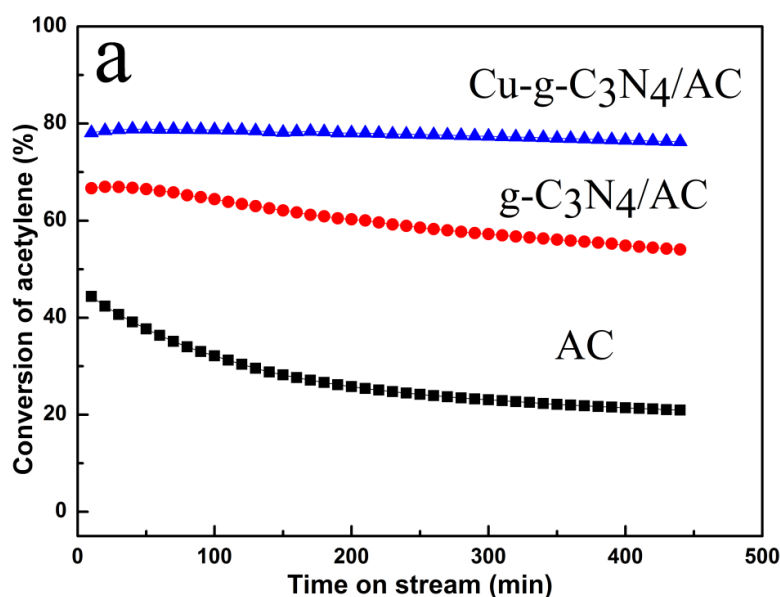


Figure 1. Cont.

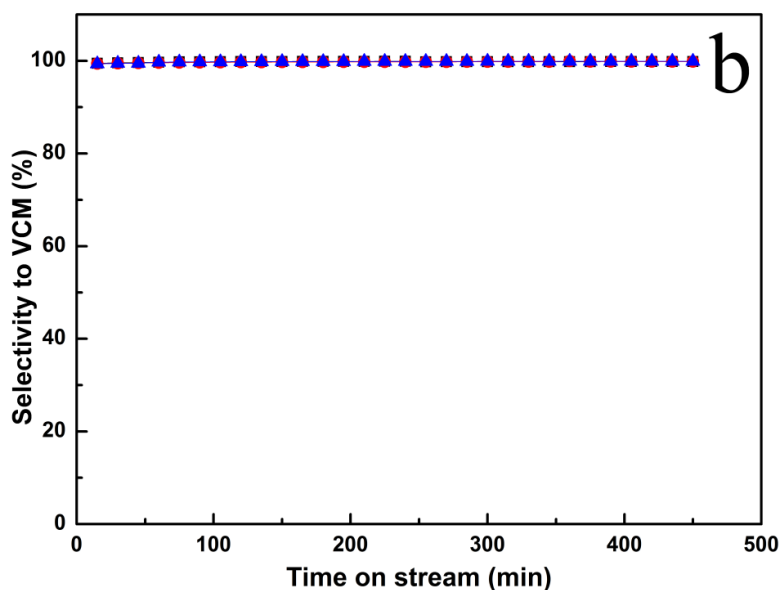


Figure 1. Catalytic performance: (a) acetylene conversion; (b) selectivity of vinyl chloride.

2.2. Transmission Electron Microscopy (TEM)

Figure 2 is the TEM image of the morphology and structure of $g\text{-C}_3\text{N}_4/\text{AC}$ and $\text{Cu-g-C}_3\text{N}_4/\text{AC}$. The layered plate junction of the $g\text{-C}_3\text{N}_4$ load on the carrier can be clearly observed, and this junction is consistent with results reported in the literature [8] (Figure 2a). Figure 2b is notably similar to Figure 2a. A layered structure was produced after CuCl_2 was added to $g\text{-C}_3\text{N}_4/\text{AC}$, which suggests that CuCl_2 did not alter the texture or structure of carbon–nitrogen compounds. The TEM elemental mapping images of $\text{Cu-g-C}_3\text{N}_4/\text{AC}$ confirm the presence of C, N, O, and Cu in the $\text{Cu-g-C}_3\text{N}_4/\text{AC}$ catalyst with homogeneously distribution (Figure 2c). Importantly, Cu and N highly overlay in the carbon structure from the elemental mapping signal, implying the presence of Cu–N coordination [9,10].

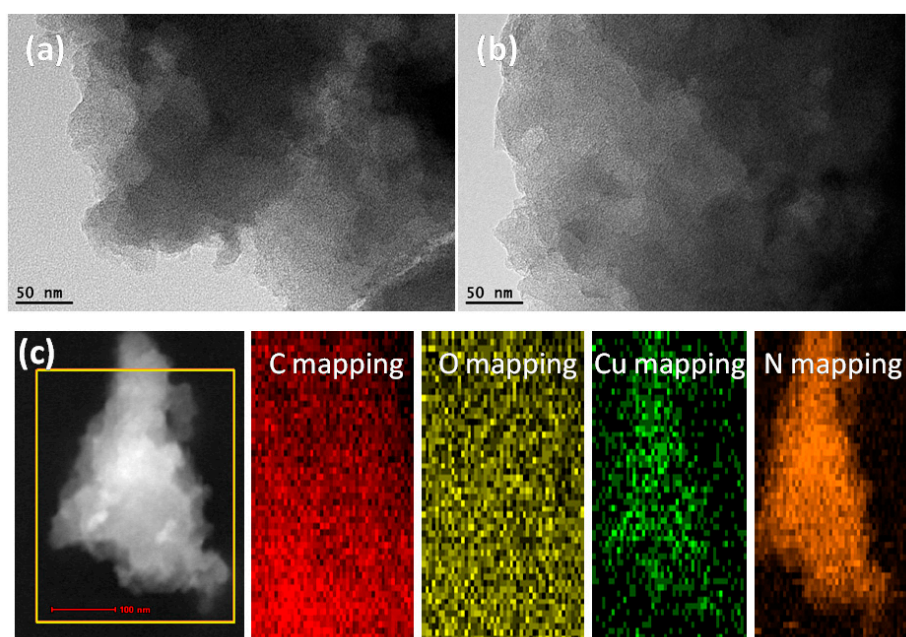


Figure 2. Transmission Electron Microscopy (TEM) micrograph of (a) $g\text{-C}_3\text{N}_4/\text{AC}$; (b) $\text{Cu-g-C}_3\text{N}_4/\text{AC}$; and (c) the TEM elemental mapping images of $\text{Cu-g-C}_3\text{N}_4/\text{AC}$.

2.3. X-ray Diffraction (XRD)

Figure 3 shows the XRD spectra of $g\text{-C}_3\text{N}_4/\text{AC}$ and $\text{Cu-}g\text{-C}_3\text{N}_4/\text{AC}$ before and after AC loading. As shown in Figure 2a, two obvious diffraction peaks at 12.9° and 27.4° were observed for $g\text{-C}_3\text{N}_4/\text{AC}$. The strong peak at 27.19° is the (002) characteristic peak for $g\text{-C}_3\text{N}_4$, which is a characteristic interplanar stacking peak of aromatic systems. The peak at 12.9° is the (100) characteristic peak for $g\text{-C}_3\text{N}_4$, which is typical of highly oriented melons [11]. The characteristic peak for the copper-modified $g\text{-C}_3\text{N}_4$ is slightly wider and weaker than that of pure $g\text{-C}_3\text{N}_4$ [12]. Notably, the XRD spectra of $\text{Cu-}g\text{-C}_3\text{N}_4/\text{AC}$ do not show the characteristic peak related to the copper element, such as that of copper or copper oxide. This observation suggests that the metal and $g\text{-C}_3\text{N}_4/\text{AC}$ formed a chemical complex (M-N) [13], which is consistent with the TEM mapping results. The two obvious characteristic peaks for AC at $2\theta = 24.4^\circ$ and 43.7° in Figure 2b, corresponding to the (002) and (101) crystal planes [14]. Moreover, the broad peaks for the $g\text{-C}_3\text{N}_4/\text{AC}$ catalysts were positively shifted when $g\text{-C}_3\text{N}_4$ was thoroughly dispersed on the support surface. A similar finding was noted with the $\text{Cu-}g\text{-C}_3\text{N}_4/\text{AC}$ catalyst.

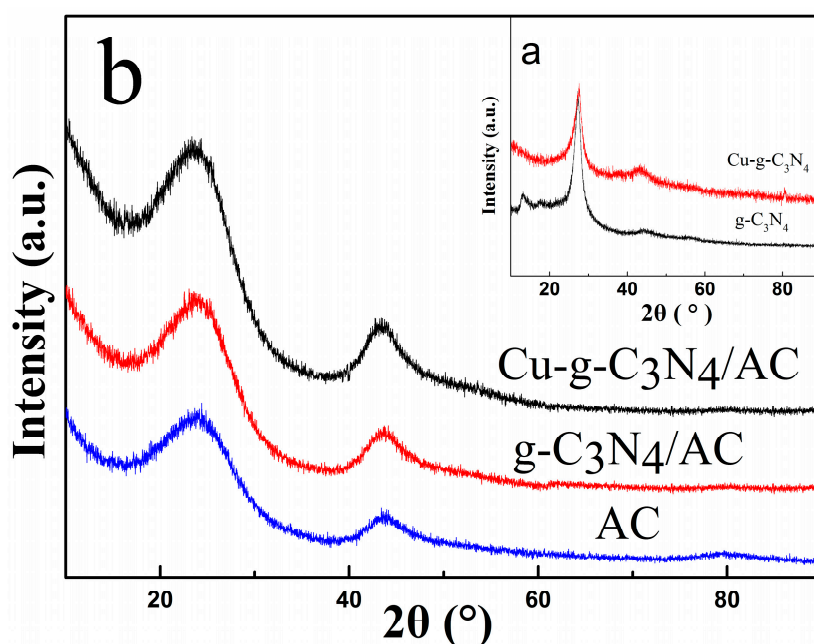


Figure 3. X-ray Diffraction (XRD) patterns: (a) $g\text{-C}_3\text{N}_4$, $\text{Cu-}g\text{-C}_3\text{N}_4$; (b) AC, $g\text{-C}_3\text{N}_4/\text{AC}$, $\text{Cu-}g\text{-C}_3\text{N}_4/\text{AC}$.

2.4. Raman Spectrum Analyses

Figure 4 shows the Raman spectroscopy of the AC, $g\text{-C}_3\text{N}_4/\text{AC}$, and $\text{Cu-}g\text{-C}_3\text{N}_4/\text{AC}$ catalysts. The I_D/I_G ratios for the AC, $g\text{-C}_3\text{N}_4/\text{AC}$, and $\text{Cu-}g\text{-C}_3\text{N}_4/\text{AC}$ catalysts are 1.097, 1.187, and 1.253, respectively. The G band of the AC was red-shifted after $\text{Cu-}g\text{-C}_3\text{N}_4$ was supported on the AC, implying that electron transfer occurs between the Cu species and the $g\text{-C}_3\text{N}_4$ matrix [15]. The Raman spectrum analysis results suggest that the Cu species are chemically coordinated to the $g\text{-C}_3\text{N}_4$ matrix.

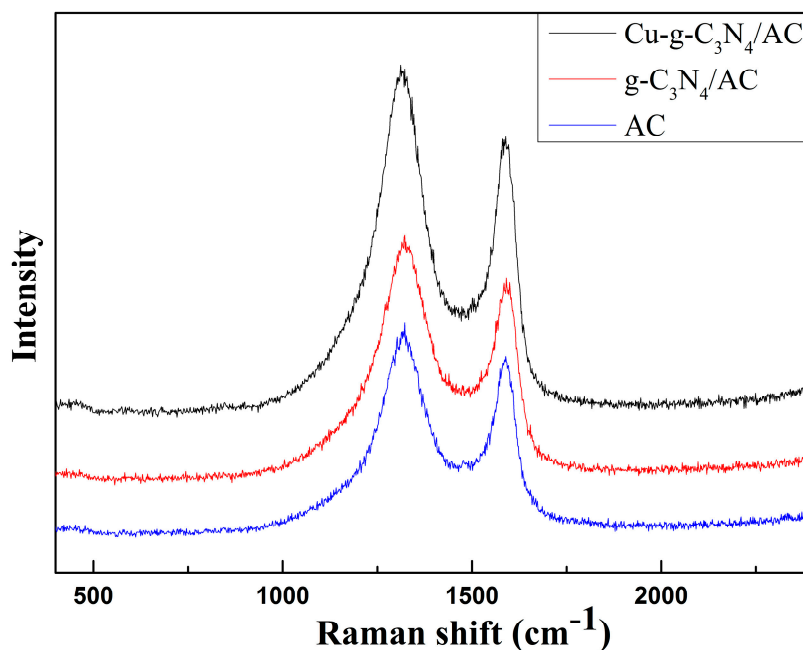


Figure 4. Raman spectra of the AC, $g\text{-C}_3\text{N}_4/\text{AC}$, and $\text{Cu-}g\text{-C}_3\text{N}_4/\text{AC}$ catalysts.

2.5. X-ray Photoelectron Spectroscopy (XPS)

The catalyst's elemental content and chemical composition, as well as the states of the nitrogen atoms in the catalysts, were characterized with XPS. The XPS results are shown in Table 1 and Figure 5. Table 1 lists the elemental contents of the AC, $g\text{-C}_3\text{N}_4/\text{AC}$, and $\text{Cu-}g\text{-C}_3\text{N}_4/\text{AC}$ catalysts. The copper content of the $\text{Cu-}g\text{-C}_3\text{N}_4/\text{AC}$ catalyst is 4.15%, which is lower than the actual value (4.3%). The nitrogen content of the $g\text{-C}_3\text{N}_4/\text{AC}$ and $\text{Cu-}g\text{-C}_3\text{N}_4/\text{AC}$ catalysts is nearly close to that listed in Table 1. The C_{1s} , N_{1s} , and O_{1s} signals were observed from the XPS survey spectrum of the $g\text{-C}_3\text{N}_4/\text{AC}$ and $\text{Cu-}g\text{-C}_3\text{N}_4/\text{AC}$ catalysts (Figure 5a), proving that C, N, and O are present in the catalyst. Furthermore, a Cu_{2p} signal was detected from the $\text{Cu-}g\text{-C}_3\text{N}_4/\text{AC}$ catalyst. The above-mentioned results show that the Cu species were successfully introduced into the $g\text{-C}_3\text{N}_4/\text{AC}$ material. The XPS deconvolution of the N_{1s} of $g\text{-C}_3\text{N}_4/\text{AC}$ and $\text{Cu-}g\text{-C}_3\text{N}_4/\text{AC}$ is shown in Figure 5b, and Table 1 presents related contents of nitrogen species of the catalyst. Graphitic N, pyrrolic N, and pyridinic N were obtained. The graphitic N corresponded to nitrogen atoms that, in the grapheme layer, linked to three carbon atoms, the pyrrolic N bonds in the five-membered rings had two carbon atoms, and the pyridinic N bonds had one p-electron localized with two carbon atoms [16,17]. The contents of pyridinic N, pyrrolic N, and graphitic N were 49.21%, 22.56%, and 28.22%, respectively (Table 2). These results indicate that pyridinic N is the main N style in the $g\text{-C}_3\text{N}_4/\text{AC}$ catalyst. For the $\text{Cu-}g\text{-C}_3\text{N}_4/\text{AC}$ catalyst, the contents of pyrrolic N increased to 40.63%, which is due to the fact that the transitional metal of Cu can promote the formation of pyrrolic N-species [18]. Related research has revealed that the type of N, particularly pyrrolic N, greatly influences the catalytic performance of catalysts in an acetylene hydrochlorination reaction. A previous investigation by our group demonstrated that pyrrolic N ranked first in the order of nitrogen species' role for this reaction [19]. Bao et al. also reported, based on experimental and theoretical results, that pyrrolic N in carbon is the active site for acetylene hydrochlorination [20]. Therefore, the pyrrolic N content of the $\text{Cu-}g\text{-C}_3\text{N}_4/\text{AC}$ catalyst increased relative to that of the $g\text{-C}_3\text{N}_4/\text{AC}$ catalyst, which is consistent with the catalytic activity.

Table 1. Elemental analysis (%) for the catalysts (XPS).

Catalyst	C	N	O	Cu
AC	88.47	0.40	11.13	–
g-C ₃ N ₄ /AC	82.15	7.30	10.55	–
Cu-g-C ₃ N ₄ /AC	78.71	7.28	9.86	4.15

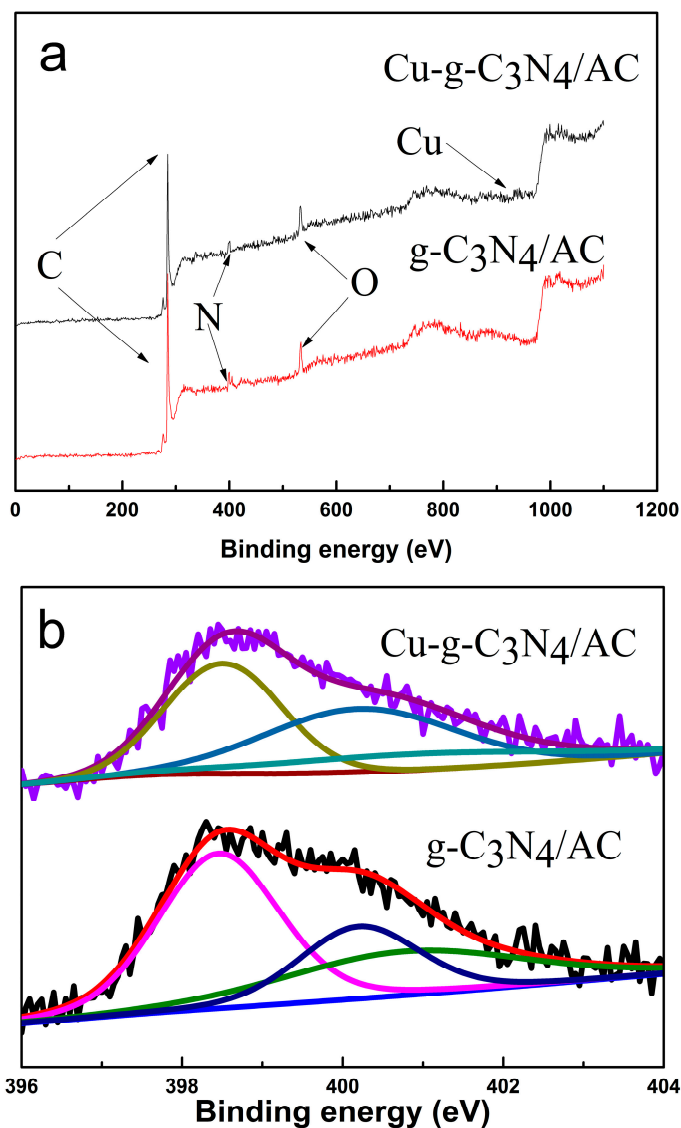


Figure 5. X-ray Photoelectron Spectroscopy (XPS) spectra of Cu-g-C₃N₄/AC and g-C₃N₄/AC: (a) Wide XPS spectrum; (b) XPS deconvolution of N_{1s}. Violet and Black: original data line; Red and Purple: fitting curve; Dark Yellow and Magenta: the characteristic peak of the pyridinic-N; Navy and Royal: the characteristic peak of the pyrrolic-N; Olive and Dark Cyan: the characteristic peak of the graphitic-N; Blue and Wine: original data.

Table 2. Relative contents and binding energies of nitrogen species of the catalysts.

Sample	Percentage of Nitrogen Type		
	Pyridinic-N	Pyrrolic-N	Graphitic-N
g-C ₃ N ₄ /AC	49.21	22.56	28.22
Cu-g-C ₃ N ₄ /AC	43.54	40.63	15.83

2.6. Temperature-Programmed Desorption (TPD)

The TPD characterization of the catalysts was conducted to analyze their adsorption of reactants (Figure 6). The desorption temperature shows the adsorption strength, and the desorption peak area is widely believed to represent the amount of adsorption. In Figure 6a, the HCl desorption temperature of $g\text{-C}_3\text{N}_4/\text{AC}$ and $\text{Cu-}g\text{-C}_3\text{N}_4/\text{AC}$ are 200.5 and 215 °C, respectively. The desorption peak area of the $\text{Cu-}g\text{-C}_3\text{N}_4/\text{AC}$ catalyst was larger than that of the $g\text{-C}_3\text{N}_4/\text{AC}$ catalyst. That is to say, the $\text{Cu-}g\text{-C}_3\text{N}_4/\text{AC}$ catalyst has a greater capacity to absorb HCl, which is consistent with its relative catalytic activity in the acetylene hydrochlorination reaction. In Figure 6b, the C_2H_2 desorption temperature of both $g\text{-C}_3\text{N}_4/\text{AC}$ and $\text{Cu-}g\text{-C}_3\text{N}_4/\text{AC}$ is 145 °C. However, the desorption peak area of the $\text{Cu-}g\text{-C}_3\text{N}_4/\text{AC}$ catalyst is smaller than that of the $g\text{-C}_3\text{N}_4/\text{AC}$ catalyst. The TPD results indicate that the CuCl_2 -modified $g\text{-C}_3\text{N}_4/\text{AC}$ catalyst improves the ability for HCl adsorption, but greatly weakens the ability for C_2H_2 adsorption.

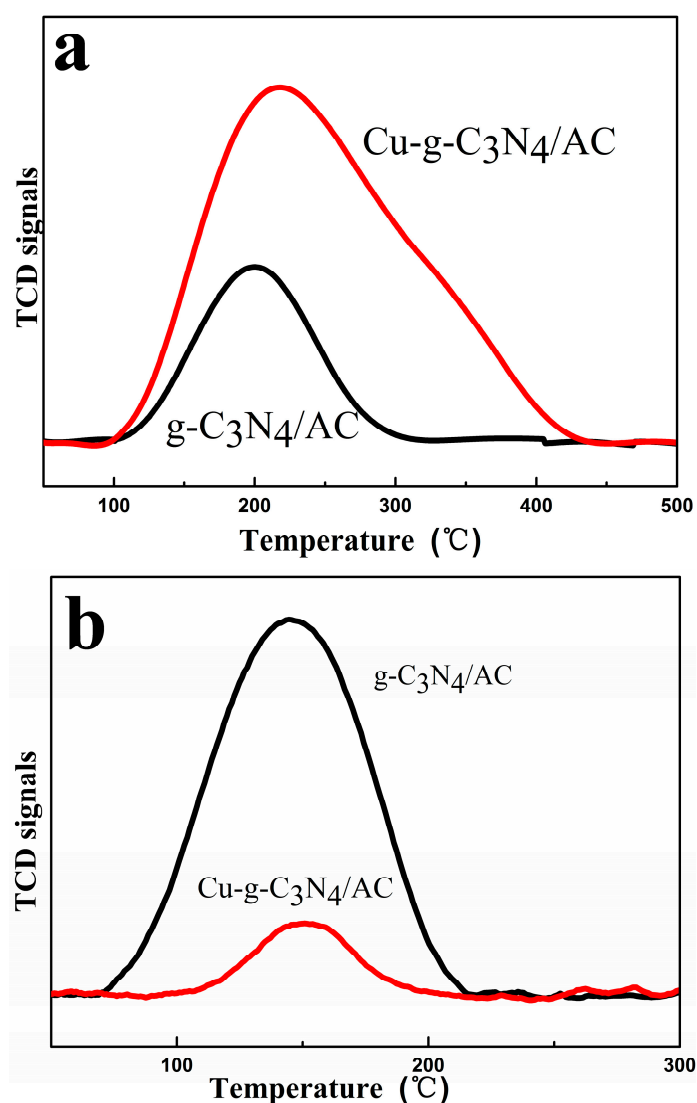


Figure 6. Temperature-programmed desorption (TPD) profiles of $\text{Cu-}g\text{-C}_3\text{N}_4/\text{AC}$ and $g\text{-C}_3\text{N}_4/\text{AC}$: (a) HCl and (b) C_2H_2 .

2.7. Low-Temperature N_2 Adsorption/Desorption Experiment (BET)

The pore structure parameters of the pores in the fresh and used catalysts are shown in Table 3. After introducing CuCl_2 to the $g\text{-C}_3\text{N}_4/\text{AC}$ catalyst, the BET surface area, the average pore diameter,

and the total pore volume of the g-C₃N₄/AC mainly decreased because the active components covered part of the space, decreasing from 857.68 to 521.26 m²·g⁻¹, and the total pore volume decreased from 0.47 to 0.29 cm³·g⁻¹. By contrast, the BET surface area and total pore volume for the Cu-g-C₃N₄/AC catalyst also decreased. This result may have been the result of the carbon deposition on the catalyst or pore [21].

Table 3. Texture parameters of the catalysts.

Sample	S _{BET} (m ² ·g ⁻¹)	V (cm ³ ·g ⁻¹)	D (nm)
g-C ₃ N ₄ /AC-Fresh	857.68	0.47	2.19
g-C ₃ N ₄ /AC-Used	521.26	0.29	2.23
Cu-g-C ₃ N ₄ /AC-Fresh	799.16	0.42	2.11
Cu-g-C ₃ N ₄ /AC-Used	475.71	0.26	2.12

2.8. Thermal Gravity Analysis (TG-DTG)

Thermal gravity analysis is conducted under oxidizing conditions, and this analysis is used to obtain information regarding carbonaceous material deposition on catalysts [22]. The extent of carbon deposition on the catalysts is shown in Table 4. The extent of carbon deposition decreased for the Cu-g-C₃N₄/AC catalyst. Specifically, the effect of Cu(II) addition on the inhibition of carbon deposition was conspicuous to some extent.

Table 4. Mass loss of the catalysts before and after reaction.

Sample	Mass Loss of Fresh Catalyst (%)	Mass Loss of Used Catalyst (%)	Amount of Carbon Deposition (%)
AC	0.34	0.94	0.60
g-C ₃ N ₄ /AC	2.23	4.27	2.04
Cu-g-C ₃ N ₄ /AC	3.64	4.17	0.53

3. Materials and Methods

3.1. Materials

The following materials were used: AC (neutral, coconut carbon, 40–60 mesh), copper(II) chloride dihydrate (CuCl₂·2H₂O, 99.8%, Aldrich, Shanghai, China), cyanamide (C₂H₄N₄, 99%, Aldrich), HCl (gas, 99%), and C₂H₂ (gas, 98%).

3.2. Catalyst Preparation

The catalysts were prepared as reported previously [12]. First, at 80 °C, dicyandiamide was mixed with deionized water, stirred for 30 min. AC was added to the above solution. Remove water by heating. The sample was calcined at 500 °C for 4 h under a flowing nitrogen atmosphere. The sample was denoted as g-C₃N₄/AC. The preparation of Cu-g-C₃N₄/AC was similar to that of g-C₃N₄/AC, but CuCl₂·2H₂O was added after dicyandiamide was mixed with deionized water.

3.3. Characterization of Physical Parameters

Low-temperature N₂ adsorption/desorption experiments on surface area and porosity were performed with a Micromeritics ASAP 2020C instrument (Micromeritics Instrument Ltd., Norcross, GA, USA). The samples were first degassed at 150 °C and analyzed at −196 °C. Raman spectrum analyses were conducted using a Raman spectrometer (Fei Tecai G2F20, FEI, Hillsboro, OR, USA) with a 633 nm Ar laser. XRD patterns were collected with a Bruker D8 advanced X-ray diffractometer (Bruker Biosciences Corporation, Billerica, MA, USA) at wide (10°–90° in 2θ) angles. TEM was used to examine the sample morphologies with a JEM2010 electron microscope (FEI, Hillsboro, OR, USA).

XPS analysis was conducted using a Kratos AXIS Ultra DLD spectrometer (Kratos, Manchester, UK). TPD was performed with a Micromeritic chemisorb 2720 (Micromeritic ASAP 2720, Micromeritics Instrument Ltd, Norcross, GA, USA). The temperature was increased from 50 to 500 °C. TG analysis of the samples was conducted with a TG DSC simultaneous thermal analyzer (NETZSCH STA 449F3 Jupiter1, Netzsch, Selb, Germany) in air. The temperature was increased from 50 to 850 °C at a heating rate of 10 °C·min⁻¹.

3.4. Catalytic Performance Evaluation

The catalytic activity tests were performed in a fixed-bed micro-reactor (internal diameter, 10 mm). Prior to the reaction, the system was purged with nitrogen gas to remove water and air for approximately 30 min. Subsequently, the catalyst was activated by passing HCl gas through the reactor. After the temperature was heated to 180 °C, C₂H₂ (2.1 mL·min⁻¹) and HCl (2.4 mL·min⁻¹) were fed into the heated reactor, which contained 2 mL of catalyst, with a GHSV of 72 h⁻¹. Gas chromatography (GC-2014C, Shimadzu, Kyoto, Japan) was used for the reaction products.

4. Conclusions

In this paper, a Cu-g-C₃N₄/AC catalyst was prepared with a simple method for an acetylene hydrochlorination reaction. The evaluation of catalytic performance showed that the Cu-g-C₃N₄/AC catalyst's catalytic performance was superior to the g-C₃N₄/AC catalyst. The introduction of CuCl₂ to the g-C₃N₄/AC catalyst increased the relative pyrrolic N content, and enhanced the adsorption capacity of HCl. Moreover, CuCl₂ inhibited coke deposition on the catalyst.

Acknowledgments: This work was supported by the National Natural Science Funds of China (NSFC, U1403294, 21666033), and the young scientific and technological innovation leader of Bingtuan (2015BC001).

Author Contributions: Mingyuan Zhu and Bin Dai designed and conceived the experiments; Wenli Zhao performed the experiments; Mingyuan Zhu analyzed the data; Bin Dai contributed reagents/materials/analysis tools; Wenli Zhao wrote the paper with direction from Mingyuan Zhu and Bin Dai; all authors participated in the analysis, interpretation, and review of the results and provided input in the writing process of the paper.

Conflicts of Interest: The authors declare no conflict of interest.

References

1. Wei, X.B.; Shi, H.B.; Qian, W.Z.; Luo, G.H.; Jin, Y.; Wei, F. Gas-phase catalytic hydrochlorination of acetylene in a two-stage fluidized-bed reactor. *Ind. Eng. Chem. Res.* **2008**, *48*, 128–133. [[CrossRef](#)]
2. Zhang, J.L.; Liu, N.; Li, W.; Dai, B. Progress on cleaner production of vinyl chloride monomers over non-mercury catalysts. *Front. Chem. Sci. Eng.* **2011**, *5*, 514–520. [[CrossRef](#)]
3. Johnston, P.; Carthey, N.; Hutchings, G.J. Discovery, development, and commercialization of gold catalysts for acetylene hydrochlorination. *J. Am. Chem. Soc.* **2015**, *137*, 14548–14557. [[CrossRef](#)] [[PubMed](#)]
4. Conte, M.; Carley, A.F.; Heirene, C.; Willock, D.J.; Johnston, P.; Herzing, A.A.; Kiely, C.J.; Hutchings, G.J. Hydrochlorination of acetylene using a supported gold catalyst: A study of the reaction mechanism. *J. Catal.* **2007**, *250*, 231–239. [[CrossRef](#)]
5. Li, X.Y.; Zhu, M.Y.; Dai, B. AuCl₃ on polypyrrole-modified carbon nanotubes as acetylene hydrochlorination catalysts. *Appl. Catal. B* **2013**, *142*, 234–240. [[CrossRef](#)]
6. Wang, X.C.; Blechert, S.; Antonietti, M. Polymeric graphitic carbon nitride for heterogeneous photocatalysis. *ACS Catal.* **2012**, *2*, 1596–1606. [[CrossRef](#)]
7. Wang, X.C.; Maeda, K.; Thomas, A.; Takanabe, K.; Xin, G.; Carlsson, J.M.; Domen, K.; Antonietti, M. A metal-free polymeric photocatalyst for hydrogen production from water under visible light. *Nat. Mater.* **2009**, *8*, 76–80. [[CrossRef](#)] [[PubMed](#)]
8. Li, X.Y.; Wang, Y.; Kang, L.H.; Zhu, M.Y.; Dai, B. A novel, non-metallic graphitic carbon nitride catalyst for acetylene hydrochlorination. *J. Catal.* **2014**, *311*, 288–294. [[CrossRef](#)]
9. Deng, L.; Zhu, M.Y. Metal–nitrogen (Co-g-C₃N₄) doping of surface-modified single-walled carbon nanohorns for use as an oxygen reduction electrocatalyst. *RSC Adv.* **2016**, *6*, 25670–25677. [[CrossRef](#)]

10. Jiang, W.J.; Gu, L.; Li, L.; Zhang, Y.; Zhang, X.; Zhang, L.J.; Wang, J.Q.; Hu, J.S.; Wei, Z.D.; Wan, L.J. Understanding the high activity of Fe–N–C electrocatalysts in oxygen reduction: Fe/Fe₃C nanoparticles boost the activity of Fe–N_x. *J. Am. Chem. Soc.* **2016**, *138*, 3570–3578. [[CrossRef](#)] [[PubMed](#)]
11. Deifallah, M.; McMillan, P.F.; Corà, F. Electronic and structural properties of two-dimensional carbon nitride graphenes. *J. Phys. Chem. C.* **2008**, *112*, 5447–5453. [[CrossRef](#)]
12. Ding, Z.X.; Chen, X.F.; Antonietti, M.; Wang, X.C. Synthesis of transition metal-modified carbon nitride polymers for selective hydrocarbon oxidation. *ChemSusChem.* **2011**, *4*, 274–281. [[CrossRef](#)] [[PubMed](#)]
13. Wang, X.C.; Chen, X.F.; Thomas, A.; Fu, X.Z.; Antonietti, M. Metal-containing carbon nitride compounds: A new functional organic–metal hybrid material. *Adv. Mater.* **2009**, *21*, 1609–1612. [[CrossRef](#)]
14. Qian, H.S.; Han, F.M.; Zhang, B.; Guo, Y.C.; Yue, J.; Peng, B.X. Non-catalytic CVD preparation of carbon spheres with a specific size. *Carbon* **2004**, *42*, 761–766. [[CrossRef](#)]
15. Yu, Q.M.; Xu, J.X.; Wu, C.X.; Guan, L.H. Strong-coupled Co-g-C₃N₄/SWCNTs composites as high-performance electrocatalysts for oxygen reduction reaction. *RSC Adv.* **2015**, *5*, 65303–65307. [[CrossRef](#)]
16. Borghei, M.; Kanninen, P.; Lundahl, M.; Susi, T.; Sainio, J.; Anoshkin, L.; Nasibulin, A.; Kallio, T.; Tammeveski, K.; Kauppinen, E.; Ruiz, V. High oxygen reduction activity of few-walled carbon nanotubes with low nitrogen content. *Appl. Catal. B* **2014**, *158*, 233–241. [[CrossRef](#)]
17. Wu, G.; Nelson, M.; Ma, S.G.; Meng, H.; Cui, G.F.; Shen, P.K. Synthesis of nitrogen-doped onion-like carbon and its use in carbon-based CoFe binary non-precious-metal catalysts for oxygen-reduction. *Carbon* **2011**, *49*, 3972–3982. [[CrossRef](#)]
18. Yan, X.H.; Xu, B.Q. Mesoporous carbon material co-doped with nitrogen and iron (Fe–N–C): High-performance cathode catalyst for oxygen reduction reaction in alkaline electrolyte. *J. Mater. Chem. A* **2014**, *2*, 8617–8622. [[CrossRef](#)]
19. Zhang, C.L.; Kang, L.H.; Zhu, M.Y.; Dai, B. Nitrogen-doped active carbon as a metal-free catalyst for acetylene hydrochlorination. *RSC Adv.* **2015**, *5*, 7461–7468. [[CrossRef](#)]
20. Li, X.Y.; Pan, X.L.; Yu, L.; Ren, P.J.; Wu, X.; Sun, L.T.; Jiao, F.; Bao, X.H. Silicon carbide-derived carbon nanocomposite as a substitute for mercury in the catalytic hydrochlorination of acetylene. *Nat. Commun.* **2014**. [[CrossRef](#)] [[PubMed](#)]
21. Zhang, H.Y.; Dai, B.; Wang, X.G.; Xu, L.L.; Zhu, M.Y. Hydrochlorination of acetylene to vinyl chloride monomer over bimetallic Au–La/SAC catalysts. *J. Ind. Eng. Chem.* **2012**, *18*, 49–54. [[CrossRef](#)]
22. Nkosi, B.; Adams, M.D.; Coville, N.J.; Hutchings, G.J. Hydrochlorination of acetylene using carbon-supported gold catalysts: A study of catalyst reactivation. *J. Catal.* **1991**, *128*, 378–386. [[CrossRef](#)]



© 2016 by the authors; licensee MDPI, Basel, Switzerland. This article is an open access article distributed under the terms and conditions of the Creative Commons Attribution (CC-BY) license (<http://creativecommons.org/licenses/by/4.0/>).